Chinese Journal of
POLYMER SCIENCE

RESEARCH ARTICLE

https://doi.org/10.1007/s10118-026-3895-z
Chinese J. Polym. Sci.

Temperature-dependent Transport of Short Peptides through Gold Plasmonic Nanopores: the Role of Charge Heterogeneity and Residue Volume

Yi Liao, Ming-Tao Lin, and Ming-Ming Ding*

School of Chemical Engineering and Light Industry, Guangdong University of Technology, Guangzhou 510006, China

Abstract Identifying complex short peptide sequences at the single-molecule level is crucial for protein sequencing. This study utilized all-atom molecular dynamics simulations to systematically examine the transport behaviors of five short peptides and their seven-lysine (Lys_7)-peptide conjugates within gold plasmonic nanopores. The results indicated that different short peptides displayed distinct characteristics in terms of conductance blockade and dwell times when subjected to an applied pulling force. Although the external pulling force significantly impacted translocation behavior and reduced the temperature's regulatory effect on conductance blockade, effective discrimination among the five short peptides was still achievable by jointly analyzing conductance blockade and dwell time. Moreover, Lys_7-peptide conjugates were created to enhance the directional transport of peptides under an electric field. Simulation results showed that, at varying applied voltages, the Lys_7-peptide systems exhibited considerable differences in translocation probability and dwell time. The translocation behavior was closely related to the strength of van der Waals interactions between the peptide segment and the gold surface, as well as the residue volume and charge state. Studies on temperature regulation further revealed that the relative conductance blockade and temperature response varied distinctly among different short peptides, exhibiting notable sequence specificity. This study demonstrates that a multiparameter identification strategy—integrating conductance blockade, dwell time, voltage dependence, temperature response, and van der Waals interactions—can effectively enhance the discrimination of complex short peptide sequences. This provides a theoretical foundation for designing gold plasmonic nanopore sensors and advancing single-molecule protein sequencing technologies.

Keywords Gold plasmonic nanopore; Molecular dynamics simulation; Temperature; Charge heterogeneity; Residue volume

Citation: Liao, Y.; Lin, M. T.; Ding, M. M. Temperature-dependent transport of short peptides through gold plasmonic nanopores: the role of charge heterogeneity and residue volume. *Chinese J. Polym. Sci.* https://doi.org/10.1007/s10118-026-3895-z

INTRODUCTION

Nanopore sequencing is a highly promising technique for analyzing single molecules. It has gained significant attention due to its high throughput, label-free detection, and exceptional sensitivity to variations in molecular structure.[1–5] For effective protein sequencing, it is essential to accurately identify and differentiate the 20 natural amino acids at the single-molecule level.[6–8] However, compared to nucleic acids, amino acids exhibit considerable differences in their side-chain structures, residue volumes, hydrophobicity, and charge properties. This complexity makes it more challenging to analyze their transport behavior in nanopores. Consequently, distinguishing between amino acids remains a significant hurdle in nanopore-based protein sequencing.[2,9,10]

Due to its unique structural advantages, gold-plasmonic nanopore sensing technology holds significant promise for single-molecule detection. A key feature of plasmonic nanopore systems is the incorporation of metallic nanostructures,[11–19] which can concentrate the optical field into nanoscale hotspots when illuminated by light.[17] In recent years, laser-induced plasmonic heating has been successfully integrated into typical experimental setups.[20–22] The localized thermal field generated by this method can regulate the behavior of biomolecules during translocation, as well as influence ion mobility, molecular conformational fluctuations, and the interaction strength between molecules and the pore wall.[11,23] For instance, Wang *et al.* developed hydrophilic porous gold structures within glass nanochannels,[18] demonstrating that plasmonic nanopores can produce strong surface-enhanced Raman scattering (SERS). Similarly, Zhao *et al.* achieved ultra-small focusing of near-infrared light within a 3 nm hotspot,[19] indicating that bowl-shaped plasmonic gold nanopores can facilitate single-molecule Raman detection in flow-based systems. Moreover, Belkin *et al.* conducted studies on the possibility of using nanoplasmonics to regulate molecular translocation through solid-state nanopores and to read sequence information using surface-enhanced Raman spectroscopy.[16] Simulations conducted by Migliore *et al.*

* Corresponding author, E-mail: mmding@gdut.edu.cn
Received August 11, 2026; Accepted September 15, 2026; Published online November 18, 2026

© Chinese Chemical Society
Institute of Chemistry, Chinese Academy of Sciences

found that the peptide translocates close to the surface of the gold nanopore,[24] where interactions between the peptide and the gold surface occur. These interactions create a frictional force that reduces the speed of peptide translocation while encouraging a more elongated conformation of the peptide. Consequently, gold-plasmonic nanopores can control molecular translocation not only through electrophoretic forces but also through localized thermal effects, thereby enhancing molecular capture rates, residence times, and identification resolution.[25,26]

Compared with conventional solid-state nanopores, gold plasmonic nanopores offer the potential for multimodal single-molecule sensing. The localized electromagnetic hotspots generated by gold nanostructures can enable SERS- or Raman-based optical detection of translocating molecules, providing complementary structural information.[12,18,19] Meanwhile, the nanopore retains electrical sensing through ionic-current and conductance-blockade measurements. In addition, peptide–gold surface interactions and plasmonic thermal effects can modulate molecular conformation, ion transport, dwell time, and translocation kinetics.[11,16,24] Therefore, the combination of optical and electrical sensing, together with controllable molecular transport, may provide richer sequence-dependent information for peptide discrimination than a single electrical signal alone.

While homopeptides are useful for studying the relationship between specific amino acid types and their translocation behavior in simulation studies,[2,27,28] their uniform composition and lack of sequence diversity make it difficult for them to accurately reflect how complex arrangements of amino acids in natural proteins influence transport dynamics. In actual protein sequences, amino acid residues with varying volumes and charge states are often distributed alternately. This leads to a significant sequence dependence in the local conformation, pore occupancy, and electric-field response of peptides in nanopores. Therefore, investigating sequence-heterogeneous short peptides can provide a more comprehensive understanding of how differences in amino acid volume, charge distributions, and thermal effects work together to regulate molecular transport through gold plasmonic nanopores under realistic protein sequencing conditions.

In this study, we investigated the transport behavior of five sequence-heterogeneous short peptides with varied residue volumes and charge states as they pass through gold plasmonic nanopores under electric-field and thermal regulation, using all-atom molecular dynamics (MD) simulations. In the present work, we mainly focus on the electrical sensing characteristics of short-peptide translocation. Due to the weak electrophoretic driving forces resulting from the low net charges of these peptides, we initially conducted steered molecular dynamics (SMD) simulations to characterize their conductance blockade signals and translocation dynamics. Building on this analysis, we designed Lys_7–peptide conjugates to enhance the electric-field response of the peptides and facilitate voltage-driven translocation through the nanopore. Further analyses of conductance blockade, dwell time, residue volume, charge distribution, and peptide–gold interactions revealed that van der Waals interactions and sequence-dependent physicochemical properties play crucial roles in regulating peptide transport. These findings highlight the significance of multiparameter analysis in nanopore-based peptide identification and provide theoretical guidance for the rational design of plasmonic nanopore sensors for single-molecule peptide and protein sequencing.

MODEL AND METHODS

Model and System Setup

We constructed a bilayer SiO_2 membrane with a thickness of 1.34 nm using Visual Molecular Dynamics (VMD). A nanopore with a radius of 0.9 nm was created by removing Si and O atoms in a ratio of 1:2. The gold bowtie structure consisted of two opposing quasi-isosceles triangles, each with a base length of 6.32 nm and a side length of 3.20 nm. The distance between the tips of the two triangles was equal to the nanopore radius, *r*, while the height of each triangle measured 2.24 nm. The geometric center of the gold bowtie was aligned with the center of the SiO_2 membrane in the *xy*-plane, and the midpoint of the bowtie gap was positioned directly above the center of the nanopore. Consequently, the nanopore axis along the *z* direction passes through the center of the bowtie gap, ensuring direct spatial coupling between the plasmonic gap region and the molecular translocation pathway. The gold plasmonic nanopore system was solvated using the modified transferable intermolecular potential with three points (TIP3P) water model based on the Chemistry at Harvard Macromolecular Mechanics (CHARMM) force field.[29] To neutralize the system and simulate an ionic solution environment, 1 mol/L KCl was added. The final simulation box has dimensions of 9.95 nm × 9.95 nm × 12.80 nm and contained approximately 1.2×10^5 atoms. The resulting all-atom model is illustrated in Fig. 1, where the K^+ and Cl^- ions are depicted as blue and red spheres, respectively.[30] This arrangement effectively divided the simulation box into two chambers: *cis* and *trans*. Consequently, only peptides, water molecules, and ions were able to pass through the nanopore.

Gold bowtie plasmonic nanopores consisting of two opposing triangular gold structures with a solid-state nanopore located in the central gap have been experimentally fabricated and investigated for molecular translocation and plasmon-assisted transport control.[11,16] Based on these experimentally established architectures, a simplified bowtie geometry was adopted in the present model. The two opposing quasi-isosceles gold triangles form a confined nanoscale tip-to-tip gap near the nanopore entrance, where plasmonic excitation can localize electromagnetic and thermal effects. By aligning the midpoint of the bowtie gap with the nanopore axis, the plasmonically active region is directly coupled to the molecular translocation pathway.

Charged Peptides

As illustrated in Fig. 2, we selected five short peptides with the following sequences: P1 (N–Tyr–Ser–Pro–Thr–Ser–Pro–Lys–Gly–Ser–Thr–C), P2 (N–Phe–Lys–Thr–Asp–Leu–Arg–Phe–Glu–Ser–C), P3 (N–Ile–Met–Asp–Glu–Val–Pro–Phe–Ser–Val–C), P4 (N–Lys–Gly–Ile–Leu–Asp–Pro–Ile–Pro–Trp–C), and P5 (N–Leu–Val–Val–Tyr–Pro–Trp–C). These sequences were based on previous research.[31] The amino acid residue volume data were also obtained from earlier studies, with volumes reported in

https://doi.org/10.1007/s10118-026-3895-z

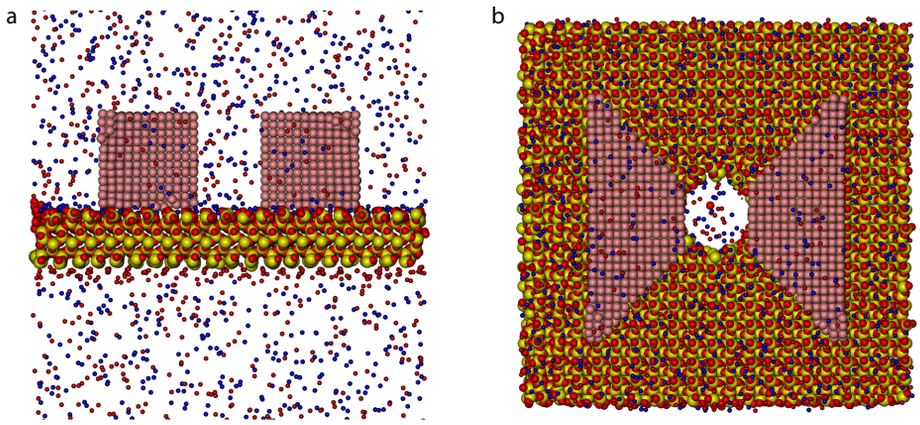


Fig. 1 Schematic illustration of the gold plasmonic nanopore system: (a) front view and (b) top view. The system consists of a nanopore with a radius of r=0.9 nm in a 1.34-nm-thick double-layer SiO_2 membrane and a gold bowtie structure positioned above the membrane. The midpoint of the bowtie gap is aligned with the nanopore center. Each gold triangle consists of 12 atomic layers, and the tip-to-tip gap is equal to r. The system is immersed in a 1 mol/L KCl electrolyte solution.

cm^3/mol.[32] The display size of each amino acid was adjusted according to its relative molecular volume. Different colors were used to differentiate between amino acid types: Tyr and Trp are shown in purple, Ser in pink, Pro in magenta, Thr in green, Lys in blue, Gly in white, Phe in yellow, Asp and Glu in red, Leu in cyan, Arg in light cyan, Ile in beige, Met in orange-yellow, and Val in light blue. The five peptides exhibit notable differences in charge distribution. Among them, P1 has an overall net charge of +1, while P3 has a net charge of −2. Conversely, P2, P4, and P5 each have a net charge of zero. Although P2 is neutral overall, its sequence includes two positively charged and two negatively charged amino acid residues. P4 contains one positively charged and one negatively charged residue, while all residues in P5 are neutral. By simulating these five peptides with varying charge distributions and volumes, we can systematically analyze the effects of charge state and residue volume on peptide transport through nanopores.

Simulation Setup and Protocols

All molecular dynamics simulations were conducted using the Groningen Machine for Chemical Simulations (GROMACS) 2022.5 package,[33] with visualization and partial post-processing analyses carried out using VMD.[34] Interatomic interactions were described using the CHARMM36 force field, in line with relevant previous studies.[33] In this work, all O atoms in SiO_2 were treated as bulk atoms rather than surface atoms. This approach preserved the charge characteristics of the nanopore as much as possible while ensuring an overall neutral charge, thus simplifying the process of adding extra ions to balance the entire system. Au atoms were modeled as neutral Lennard-Jones particles using established parameters for metallic surfaces.[35] The Lorentz-Berthelot combination rules were applied to describe interactions between nonbonded atoms. The SETTLE and RATTLE algorithms were used to constrain the geometry of water molecules and other covalent bonds involving hydrogen atoms.[36] The cutoff distance for van der Waals (vdW) interactions and short-range electrostatic interactions was set to 12 Å. Long-range electrostatic interactions were handled using the particle mesh Ewald (PME) method.[37] Throughout the simulations, a harmonic potential of 1000 kJ/mol/nm^2 was applied to restrain the positions of the gold bowtie and the SiO_2 membrane, thereby maintaining the structural stability of the plasmonic nanopore system.

All simulation trajectories were integrated using the leap-frog algorithm with a time step of 1 fs, and data were recorded every 5 ps for subsequent analysis. Periodic boundary conditions (PBCs) were applied in all three directions: x, y, and z. Initially, each system underwent energy minimization using the steepest descent algorithm for up to 1×10^4 steps. The system was then equilibrated for 50 ns under the constant-particle-number, pressure and temperature (NPT) ensemble to achieve a stable configuration with minimal fluctuations in box size over an extended period. The pressure was maintained at 100 kPa by semi-isotropically adjusting the system dimensions along the z axis, which corresponds to the nanopore direction, using the Berendsen barostat.[38] This ensured proper relaxation of both density and pressure. The gold bowtie structure consisted of 12 layers. For all systems requiring temperature control, the velocity-rescale thermostat with a time constant of 0.2 ps was specifically applied to regulate the temperature of the lower six layers of the gold bowtie.[39] This configuration generated strong localized thermal perturbations near the gold nanostructure, which are essential for investigating thermally modulated transport. Previous simulation studies of plasmonic systems support the use of localized heating.[40] Furthermore, the analysis of thermal equilibration illustrates that these localized thermal hotspots swiftly create a uniform temperature field within the confined nanopore environment.[30] In contrast, no temperature control was applied to the other components of the system. Following this, the system underwent an additional 30 ns of equilibration under the constant-particle-number, volume and temperature (NVT) ensemble to further stabilize the temperature and prepare for production simulations.

After equilibration, the restraints on the peptide atoms were removed. In the NVT ensemble, a uniform and constant electric field, $E=(0, 0, E_z)$, was applied in the direction perpendicular to the membrane, specifically along the z direction of the system. To further investigate how the strength of the electric field affects the transport behavior of short peptides, five different electric-field strengths were tested: 0.3, 0.5, 0.75,

https://doi.org/10.1007/s10118-026-3895-z

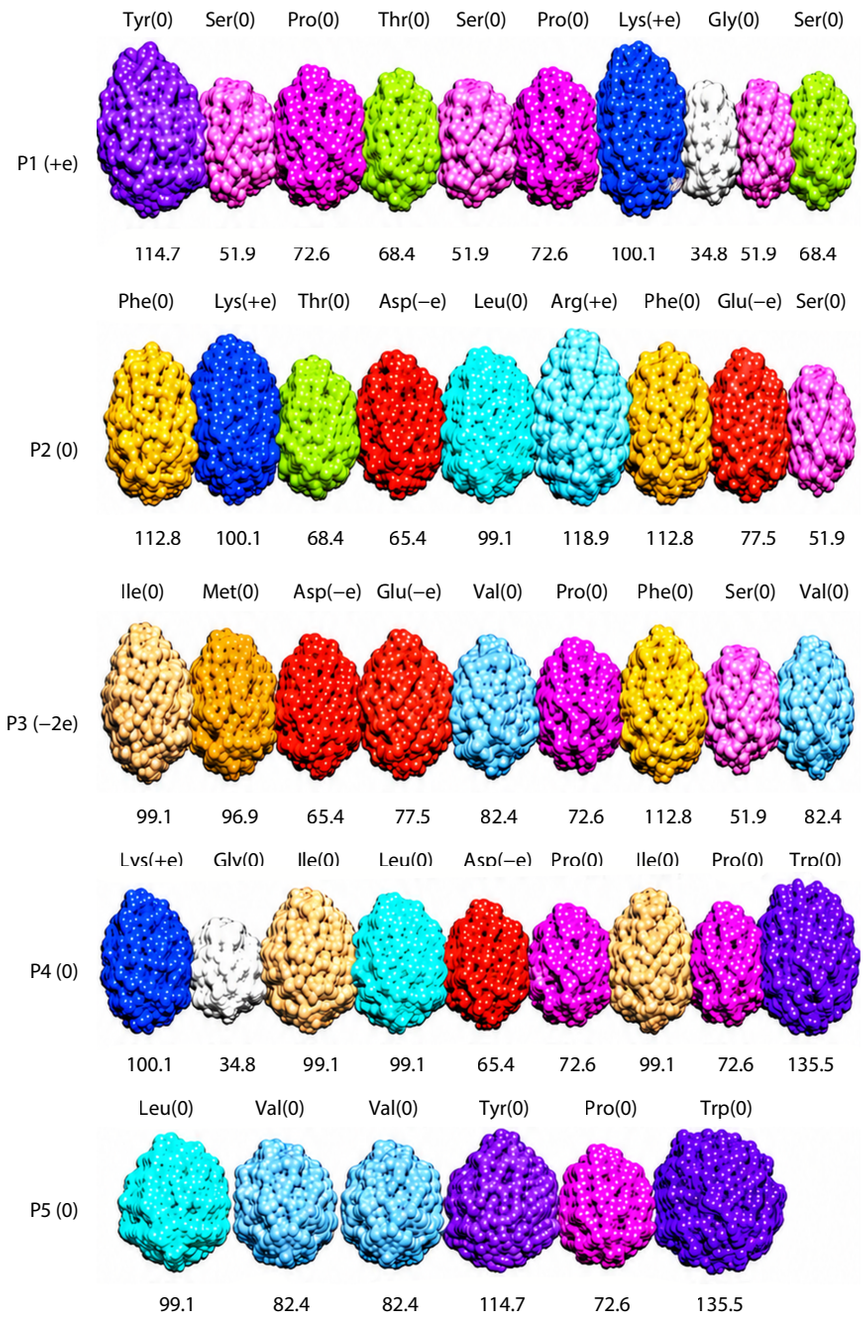


Fig. 2 Five short peptides (P1–P5) exhibit varying charges and residue volumes. The amino acid residue volume data were obtained from a previous report, with the volumes expressed in cm^3/mol. The size of each amino acid is displayed according to its relative molecular size, and different colors are used to represent the various types of amino acids.

1.0, and 1.5 V/nm. The temperature range of 298.15–373.15 K was selected with reference to previous studies of locally heated and thermally modulated nanopore systems.[21,30,37] Because the short peptides considered here do not possess a well-defined folded tertiary structure comparable to that of larger proteins, increasing temperature mainly affects their conformational fluctuations, molecular mobility, and peptide–gold interactions rather than inducing conventional protein thermal denaturation. For the electric field, previous molecular dynamics simulations of polypeptide transport through gold nanopores employed longitudinal electric-field strengths of approximately 0.25–1.0 V/nm.[24] Accordingly, electric-field strengths of 0.3, 0.5, 0.75, and 1.0 V/nm were selected as comparable conditions, while 1.5 V/nm was additionally included to examine strongly driven translocation within the accessible MD simulation timescale. Additionally, SMD simulations were included in some of the calculations. Using the center of mass of the SiO_2 membrane as the coordinate origin, a harmonic potential with a spring constant of 1000 kJ/mol/nm^2 was applied to the first residue at the N-terminus of the short peptide. The peptide was pulled at a constant velocity of 0.1 nm/ns through the gold plasmonic

https://doi.org/10.1007/s10118-026-3895-z

nanopore along the direction connecting it to the center of mass of the SiO_2 membrane. Production simulations lasting between 20 and 100 ns were conducted for each system to ensure adequate sampling of translocation events. For each simulation condition, 3–15 independent MD trajectories were performed using independently initialized simulations to account for event-to-event variations in peptide translocation. The dwell-time statistics were obtained from the successful translocation events under each condition, and the error bars reflect event-to-event variability among the independent trajectories.

The blockade current is the most critical variable for identifying charged amino acids. When ions pass through the nanopore, the ionic current $I(t)$ can be calculated by determining the number of ions crossing the nanopore, as expressed below (Eq. 1):[41]

$$I(t) = \frac{1}{\Delta t L_z} \sum_{i=1}^{N} q_i [Z_i(t + \Delta t) - Z_i(t)] \quad (1)$$

where Z_i and q_i represent the coordinate along the z direction and the charge of the i^{th} ion, respectively. Here, $\Delta t = 5$ ps denotes the time interval, and N is the total number of ions. The charges of K^+ and Cl^- ions are given as $q_K = +e$ and $q_{Cl} = -e$, respectively. $Z_i(t)$ indicates the coordinate of the ion at time t, and L_z represents the length of the simulation system along the z direction.[42]

Under the same applied electric-field strength and system dimensions, the effective potential difference across the nanopore remains unchanged. Since $G=I/V$, the relative conductance change is equivalent to the relative ionic-current change, *i.e.*, $(G_b-G_0)/G_0=(I_b-I_0)/I_0$. Therefore, $(I_b-I_0)/I_0$ is used to characterize the relative conductance blockade in this study.[43,44]

RESULTS AND DISCUSSION

Translocation of Short Peptides

Initially, we aligned the center of mass of each short peptide with the geometric center of the nanopore, positioning it 2 nm above the pore entrance along the z axis. Prior to the application of an electric field, the nitrogen atom at the peptide's terminus was restrained while all other atoms were permitted to freely explore their conformational space. The simulation results indicated that none of the five short peptides achieved complete translocation. The five peptides exhibit distinct charge distributions and relatively low net charges. Specifically, P1 and P3 have net charges of +1 and −2, respectively, whereas P2, P4, and P5 are electrically neutral. Under a unidirectional uniform electric field, the electrophoretic response of each peptide depends on its charged residues and overall charge distribution. Consequently, the resulting driving force is insufficient for these short peptides to overcome the interaction and steric barriers within the nanopore and achieve complete spontaneous translocation under the investigated conditions. The steered molecular dynamics setup is shown in Fig. 3.

Under the same simulation conditions, a harmonic potential with a force constant of 1000 kJ/mol/nm^2 was applied to the first residue at the N-terminus of each short peptide to assist in peptide translocation by pulling, as illustrated in Fig. 3. The short peptide was pulled through the nanopore along

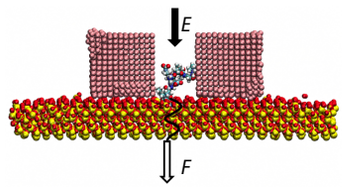


Fig. 3 Schematic diagram for the SMD simulation. The center of mass of the peptide P3 is located 2 nm above the pore entrance, precisely at the geometric center of the pore along the z axis. Before the electric field is applied, the nitrogen atom at the terminus of the peptide is restrained. Once the constraints are released, both an electric field and an external pulling force are applied simultaneously.

the z axis at a constant velocity of 0.1 nm/ns, allowing us to characterize the blockade variation induced by peptide translocation through the nanopore. To facilitate observation of the changes in pulling force, the force was averaged over 1 ns intervals. In Fig. 4, the left vertical axis represents the applied pulling force, depicted as the blue curve. A positive pulling force indicates the expected pulling direction, which is downward and consistent with the direction of peptide translocation through the nanopore. A negative value indicates resistance in the opposite direction. At the start of the simulation, a pulling force drove the short peptide toward the entrance of the nanopore. Once the peptide entered the nanopore, the pulling force increased rapidly, allowing the peptide to overcome the energy barrier and escape from adsorption on the gold bowtie structure. The first positive peak in the force profile corresponds to the peptide-entry stage, during which the peptide overcomes the energy barrier near the nanopore entrance. As the main body of the short peptide gradually enters the nanopore, the required pulling force

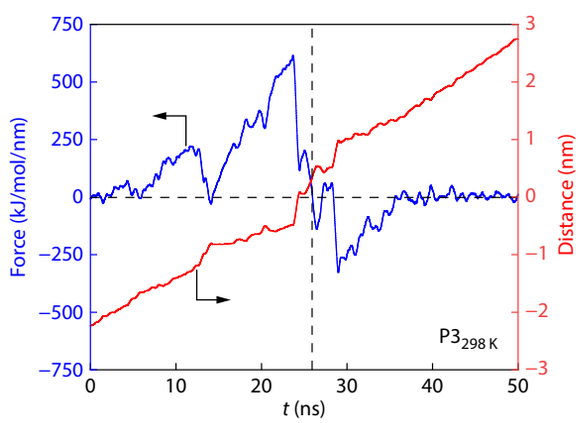


Fig. 4 Pulling force and the center-of-mass position of peptide P3 at 298 K as a function of time. The left y-axis displays the applied force (represented by the blue line) over time, which is used to pull the peptide through the nanopore at a constant speed. Positive force values indicate the direction of pulling (downward) and align with the translocation direction of the peptide, while negative values denote the opposing direction. The maximum and minimum force values correspond to the moments when the peptide enters and exits the nanopore, respectively. Meanwhile, the right y-axis presents the distance between the center of mass of the short peptide and the center of the nanopore, which is represented by the red line.

decreases. The subsequent negative valley corresponds to the peptide-exit stage. The right vertical axis displays a red curve that tracks the time-dependent distance between the center of mass of the peptide and the center of the nanopore. As the peptide was pulled toward and into the nanopore, this distance decreased. Subsequently, as the peptide exited on the other side, the distance increased. Notably, abrupt changes in the direction of the pulling force caused sudden fluctuations in the position of the short peptide. Additionally, continuous thermal collisions with solvent molecules disrupted smooth linear motion, resulting in oscillations in the center-of-mass distance curve between the two force extrema.

We systematically quantified the conductance changes induced by five short peptides. As shown in Fig. 5(a), each peptide exhibited distinct relative conductance blockade values, suggesting that they can generate unique, sequence-dependent conductance fingerprints. However, due to the overlap of the error bars for the blockade values of the different peptides, it was challenging to clearly differentiate all five peptides using a single blockade parameter.

We conducted a further analysis of the dwell times of five short peptides under identical electric field conditions, as illustrated in Fig. 5(b). The dwell times for the different peptides showed significant variations. Analyzing the volume and charge distribution of the amino acid residues revealed that the differences in conductance blockade and dwell time among the peptides are closely related to their sequence characteristics. For instance, peptide P1 has the smallest average amino acid residue volume among the five peptides, which results in both a relatively low conductance blockade and a shorter dwell time. In contrast, peptide P5 has a larger average residue volume, leading to a stronger conductance blockade. However, because P5 has the fewest amino acid residues and the shortest overall chain length, its dwell time remains relatively short. Peptides P3 and P4 exhibit notable conductance blockades during translocation due to peptide chain distortion and folding that occur as a result of their charge states and interactions with the nanopore. This distortion, however, leads to shorter dwell times. On the other hand, peptide P2 contains the highest number of charged amino acid residues, which enhance its interactions with the gold nanopore. As a result, P2 experiences greater hindrance during translocation and, therefore, has a longer dwell time.

We also investigated how temperature affects the conductance blockade of short peptides. Our SMD simulations showed that temperature variations had little to no significant impact on the conductance blockade of these peptides. This is primarily because the externally applied pulling force was the main factor driving the peptide translocation process. While increasing the temperature can enhance ion mobility and reduce interaction times, these effects were not clearly observable in the blockade signals.

Translocation of Peptide-peptide Conjugates

To address the challenge of insufficient net charge, which can impede effective translocation in a unidirectional electric field, previous studies have sought to improve the electric-field responsiveness of target peptides by covalently attaching charged groups. For instance, Yan *et al.* developed peptide-oligonucleotide conjugates and utilized nanopore-induced phase-shift sequencing to measure them, successfully allowing direct observation of ratcheting motion along the peptide chains.[45] Similarly, Chen *et al.* used helicase-controlled single-stranded deoxyribonucleic acid (ssDNA)-peptide conjugates that translocated through a Mycobacterium smegmatis porin A (MspA) nanopore, achieving read lengths of up to 17 amino acids.[46] This demonstrated the capability to differentiate between amino acid residues with varying charges, as well as to identify phosphorylation sites. Additionally, Chen *et al.* employed an ssDNA-peptide strategy to examine the translocation process, effectively stretching the peptide chain and enabling the identification of distinct spike-like signals.[47] Ouldali *et al.* conjugated amino acids with a seven-arginine (Arg_7) peptide,[6] significantly enhancing the electrophoretic driving force under an applied electric field and promoting rapid translocation into the nanopore.

Inspired by these studies, we have proposed a novel molecular design strategy: a homopeptide composed of seven lysine residues was covalently attached to the N-terminus of each short peptide, resulting in the formation of Lys_7-peptide conjugates, as illustrated in Fig. 6. All other parameters remain consistent with those described in the previous section. Lysine is positively charged under physiological condi-

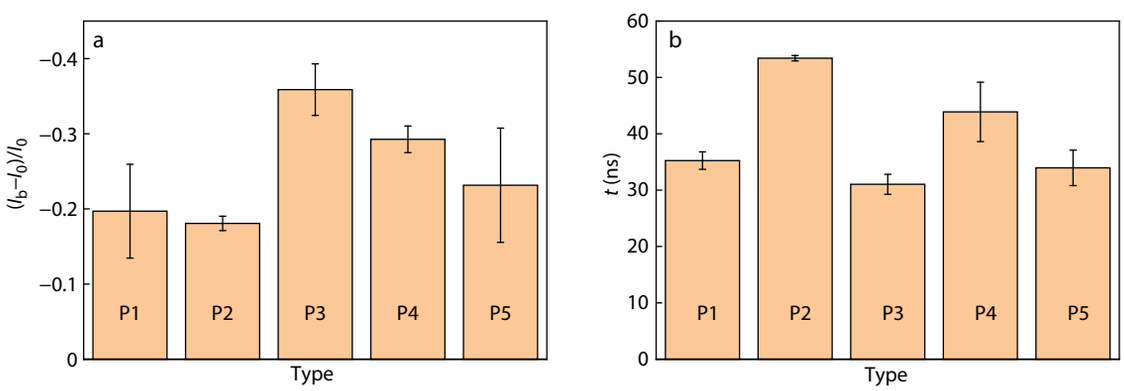


Fig. 5 (a) Relative conductance blockade of the five short peptides, calculated using the formula $(I_b-I_0)/I_0$, where I_b is the blocked current and I_0 is the baseline current. Since peptide occupation reduces the ionic current ($I_b<I_0$), the relative conductance blockade values are negative, and a larger absolute value indicates a stronger conductance blockade; (b) Dwell time for each peptide, which is defined as the duration of the simulation that elapses from when the first atom enters the nanopore at the N-terminus until the last atom exits the nanopore at the C-terminus.

https://doi.org/10.1007/s10118-026-3895-z

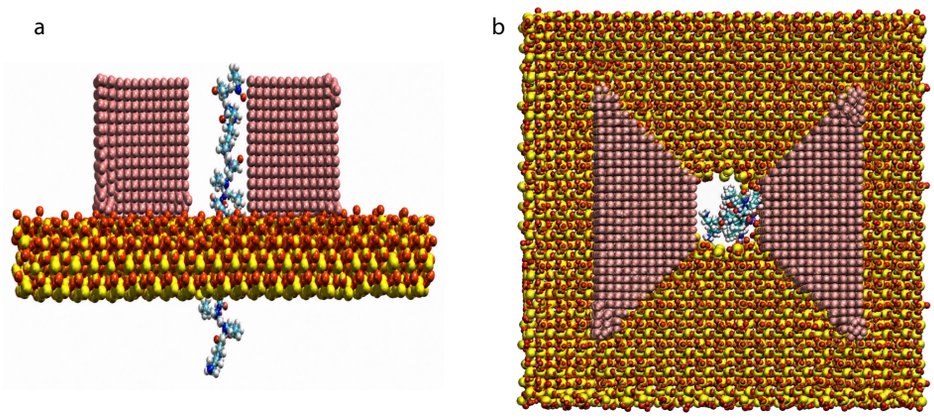


Fig. 6 Simulation setup for the translocation of Lys_7-peptide conjugates: (a) main view and (b) top view. The N atom at the peptide terminus is restrained before the application of the electric field, while all other atoms remain in a free conformation.

tions, which allows it to impart a stable positive charge to short peptides that initially possess an insufficient net charge, thereby generating an adequate electrophoretic driving force. This design not only retains the sequence complexity of the original short peptides but also enhances the efficacy of electric-field-driven translocation by incorporating a homopeptide "pulling tag".

We conducted a systematic investigation of the translocation probabilities of Lys_7–peptide conjugates under various voltage-driven conditions, as detailed in Table 1. The results indicate that different short peptides respond differently to voltage electric fields. For instance, P1 and P5 exhibited translocation events even at a relatively low electric field of −0.3 V/nm. In contrast, P3 required a much stronger electric field of −1.5 V/nm to achieve translocation. Notably, while the main body of peptides P2 and P4 began to enter the nanopore at electric-field strengths of −0.5 V/nm and −0.75 V/nm, respectively, neither peptide completed the translocation event during the simulations.

Table 1 Translocation probabilities of the Lys_7-peptide conjugates at various voltages.

Voltage (V/nm)	P1	P2	P3	P4	P5
−0.3	0.875	0	0	0	1
−0.5	1	0	0	0	1
−0.75	1	0	0	0	1
−1.0	1	1	0.2	1	1
−1.5	1	1	0.8	1	1

Since the gold atoms were considered electrically neutral, electrostatic interactions between the gold nanopore and the peptide were not included, and only van der Waals interactions were taken into account. Fig. 7 illustrates the vdW interaction energies between five short peptides and the gold nanopore. The sign of the vdW interaction energy indicates whether the peptide–gold interaction is attractive or repulsive, with negative and positive values corresponding to attractive and repulsive interactions, respectively. The absolute value reflects the interaction strength, with a larger absolute value indicating a stronger interaction. The results reveal that peptides P1 and P5 exhibit relatively weak vdW interactions, which accounts for their ability to translocate even under low-voltage conditions. In contrast, P3 displays the strongest vdW attraction, indicating that it must overcome a higher energy barrier during translocation, thus requiring the highest driving voltage. Peptides P2 and P4 show intermediate interaction energies, and their translocation behaviors follow a gradual, voltage-dependent trend. These findings suggest that the introduction of charged groups allows Lys_7-peptide conjugates to undergo voltage-regulated translocation. Furthermore, the probability of translocation is closely related to the peptide sequence. The vdW interactions significantly influence the energy barrier and the necessary voltage threshold, playing a crucial role in regulating peptide translocation behavior.

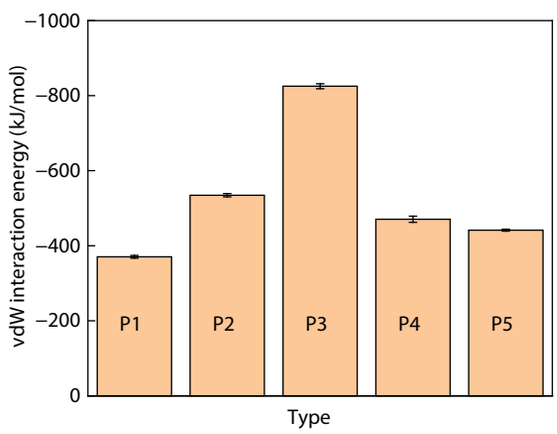


Fig. 7 vdW interaction energies between the Lys_7-peptide conjugates and the gold nanopore.

We further analyzed the dwell times of the Lys_7-peptide conjugates at different voltages, as summarized in Table 2. The data show a significant decrease in the dwell time of all short peptides as the voltage increased, indicating that the enhanced electrophoretic force effectively speeds up peptide translocation. For instance, P1 had an average dwell time of 5.68 ns at −0.3 V/nm. However, when the voltage rose to −1.5 V/nm, the dwell time dramatically dropped to 0.09 ns, representing a reduction of nearly two orders of magnitude. This indicates that a higher voltage generates a stronger electrophoretic force on the positively charged Lys_7 segment, fa-

https://doi.org/10.1007/s10118-026-3895-z

Table 2 Dwell times of the Lys_7-peptides at various applied voltages. [a]

Voltage (V/nm)	P1	P2	P3	P4	P5
−0.3	5.68±1.83	–	–	–	18.81±17.03
−0.5	0.90±0.38	–	–	–	1.63±0.53
−0.75	0.32±0.08	–	–	–	0.40±0.10
−1.0	0.15±0.02	0.64±0.23	12.20	28.92±7.98	0.30±0.12
−1.5	0.09±0.02	0.27±0.02	5.48±4.08	1.19±0.59	0.19±0.07

[a] "–" indicates that no translocation occurred. Values are given in ns.

cilitating a quicker translocation of the entire short peptide through the nanopore. Interestingly, at the same voltage, the dwell times varied significantly among the different short peptides. For example, at −1.0 V/nm, the dwell time for P1 was only 0.15 ns, while P3 and P4 had dwell times of 12.20 and 28.92 ns, respectively. This variation can be attributed to the differences in vdW interactions, as shown in Fig. 7. P1 interacts weakly with the gold surface, which results in lower translocation resistance and allows for a rapid passage through the nanopore. In contrast, P3 and P4 exhibit stronger vdW attractions, leading to a stronger adhesion between the peptide and the pore wall during translocation, thereby resulting in longer dwell times.

We further examined how temperature affects the relative conductance blockade of the Lys_7-peptide conjugates at an applied voltage of −1.0 V/nm. The results are presented in Fig. 8. Overall, as the temperature increased from 298.15 K to 373.15 K, the blockade characteristics and temperature responses of different short peptides showed notable differences.

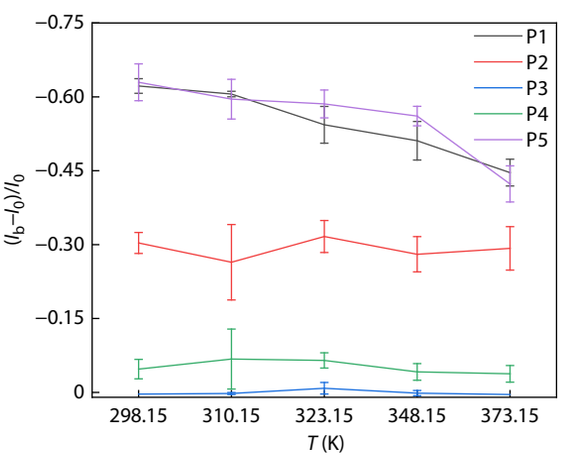


Fig. 8 Temperature dependence of the relative conductance blockade $(I_b - I_0)/I_0$ for the Lys_7-peptide conjugates under an applied voltage of −1.0 V/nm.

As discussed in a previous study,[31] the uniformity of the signal and the depth of the blockade in peptides are primarily influenced by their charge properties and the distribution of hydrophobic residues. Positively charged peptides, such as P1, tend to adopt stable, extended conformations under the influence of an electric field, resulting in uniform blockade signals with relatively high amplitudes. In contrast, negatively charged peptides like P3 experience an electrophoretic force that opposes the direction of translocation. Consequently, they tend to remain near the center of the pore and produce very shallow blockade events with broader signal distributions. On the other hand, neutral peptides that are rich in aromatic residues, such as P5, may tightly occupy the pore cross-section through hydrophobic interactions or dimer formation, leading to deep blockade signals.

Our simulation results showed that P1, which contains a single lysine residue, exhibited a high blockade value above −0.45 at low temperatures. This value decreased smoothly with increasing temperature, indicating its conformational stability. In contrast, P2, which has a balanced mix of positive and negative charges, displayed large fluctuations in the blockade signal due to the presence of internal negatively charged residues, leading to conformational polymorphism. P3, which contains two negatively charged residues, showed an extremely low blockade value below −0.1 because it tended to remain suspended near the center of the nanopore. P4, a hydrophobic and amphipathic peptide, also exhibited weak blockade due to its compact conformation. Finally, P5, which is fully neutral, demonstrated a high blockade value above −0.45, attributed to hydrophobic and aromatic interactions. These findings suggest that the sequence composition of the peptides influences both the amplitude of the conductance blockade and its response to temperature by regulating peptide conformation and the mode of pore occupancy during translocation.

At an applied voltage of −1.0 V/nm, we calculated the dwell times of the Lys_7-peptide conjugates at different temperatures, and the results are summarized in Table 3. The findings indicate that the dwell times of P1 and P5 consistently fluctuated within the range of 0.1–0.3 ns. This suggests that thermal perturbations have a limited effect on the translocation rates of these two peptides, with their dynamics primarily governed by the electrophoretic force rather than thermal motion. In contrast, the dwell time of P2 fluctuated within a relatively narrower range of 0.57–1.19 ns as the temperature increased. This behavior reflects its sequence characteristics, which feature a balance of positive and negative charges. Temperature variation may induce rearrangements of intramolecular electrostatic interactions within the short peptide, moderately influencing its translocation rate. However, no significant change was observed overall.

Notably, the dwell times of P3 and P4 exhibited pronounced, temperature-dependent, nonmonotonic behavior. This phenomenon may be attributed to two potential factors. First, increasing temperature enhances molecular thermal motion, helping to overcome interaction energy barriers within the nanopore and thereby accelerating translocation. Second, elevated temperatures may lead to conformational rearrangements of the peptides. Within certain temperature ranges, transient conformations more favorable for interac-

https://doi.org/10.1007/s10118-026-3895-z

Table 3 Dwell times of the Lys_7-peptide conjugates at various temperatures under an applied voltage of −1.0 V/nm. [a]

Temperature (K)	P1	P2	P3	P4	P5
298.15	0.15±0.02	0.64±0.23	12.29	28.92±7.98	0.30±0.12
310.15	0.15±0.01	1.19±0.37	72.28±31.80	38.58±3.62	0.22±0.02
323.15	0.15±0.02	0.99	91.93±9.43	16.54±16.82	0.11±0.01
348.15	0.13	0.80±0.08	47.45±34.34	5.01±2.35	0.12±0.03
373.15	0.018±0.02	0.57±0.19	34.34	26.11±18.36	0.11±0.04

[a] Values are given in ns.

tions with the gold surface may form, which could increase dwell time. The competing effects of thermally enhanced barrier crossing and conformation-dependent peptide–gold interactions vary among independently initialized trajectories. Consequently, some translocation events proceed relatively rapidly, whereas others experience transient retention near the gold surface, resulting in a broader distribution of dwell times and relatively large error bars for P3 and P4 at several temperatures. This finding further emphasizes that relying solely on the dwell time at a single temperature may be insufficient to distinguish between all peptide sequences. In contrast, a multiparameter identification strategy that combines relative conductance blockade, interaction energy, and dwell time can effectively enhance the resolution of complex peptide sequences. Lin *et al.* demonstrated that two model peptides with the same amino acid compositions but different sequence arrangements resulted in distinct blockade amplitudes and dwell times when tested in an aerolysin nanopore.[48] Molecular dynamics simulations revealed that these differences were due to variations in hydrogen bonding, conformational extension, and peptide–nanopore interactions, rather than differences in molecular mass. These findings align with the deviations of P2–P4 from the simple volume–blockade relationship observed in our study.

CONCLUSIONS

This study addresses the challenge of identifying complex amino acid sequences in natural proteins by selecting five short peptides with varying charge characteristics as model systems. All-atom MD simulations were employed to systematically investigate the temperature-dependent transport behavior of these peptides in gold plasmonic nanopores. The results indicated that the five peptides exhibited distinct charge distributions, with net charges of +1, 0, −2, 0, and 0 for P1–P5, respectively. Under the investigated unidirectional electric-field conditions, none of the five peptides could spontaneously complete translocation through the nanopore. Therefore, SMD simulations were subsequently employed to assist peptide translocation. Different short peptides exhibited unique characteristics concerning conductance blockade and dwell times under the applied pulling force. Although the external pulling force largely influenced translocation behavior and diminished the regulatory effect of temperature on conductance blockade, effective discrimination among the five sequence-heterogeneous short peptides was still achieved by jointly analyzing conductance blockade and dwell time. This confirms the feasibility of utilizing a multiparameter approach for the identification of complex short peptides.

Additionally, Lys_7-peptide conjugates were constructed to enhance the directional transport of peptides under an electric field. Simulation results revealed that, at varying applied voltages, the Lys_7-peptide systems demonstrated significant differences in translocation probability and dwell time. Their translocation behavior was closely linked to the strength of vdW interactions between the peptide segment and the gold surface, as well as to residue volume and charge state. Temperature regulation studies further indicated that the relative conductance blockade and temperature response of different short peptides exhibited notable sequence specificity. Additionally, the temperature dependence of the dwell time indicated that P1 and P5 were relatively unaffected by thermal variations, while P3 and P4 demonstrated non-linear temperature responses. This highlights the complex interactions between peptide conformation and intermolecular forces.

This study significantly enhances our understanding of the physical transport mechanisms of complex short peptides through gold plasmonic nanopores. It also lays the groundwork for developing a multiparameter protein identification system that combines conductance blockade, dwell time, volume effects, and charge response. The conductance blockade is governed by multiple parameters, including volume effects, charge response, and conformation. The findings indicate that relying on a single electrical signal parameter is inadequate for fully capturing the structural and sequence variations of complex short peptides. In contrast, a multiparameter joint analysis can significantly improve our ability to differentiate between various peptides. This research offers new insights and design strategies for advancing nanopore-based technologies for protein sequencing and may also provide a useful basis for future studies on the identification of post-translational modifications.

Conflict of Interests

The authors declare no interest conflict.

Data Availability Statement

The related data of this paper is data that should not be shared, and can be obtained from the author for reasonable reasons. The author's contact information: mmding@gdut.edu.cn.

ACKNOWLEDGMENTS

This work was financially supported by the National Natural Science Foundation of China (Nos. 22227804 and 22373025).

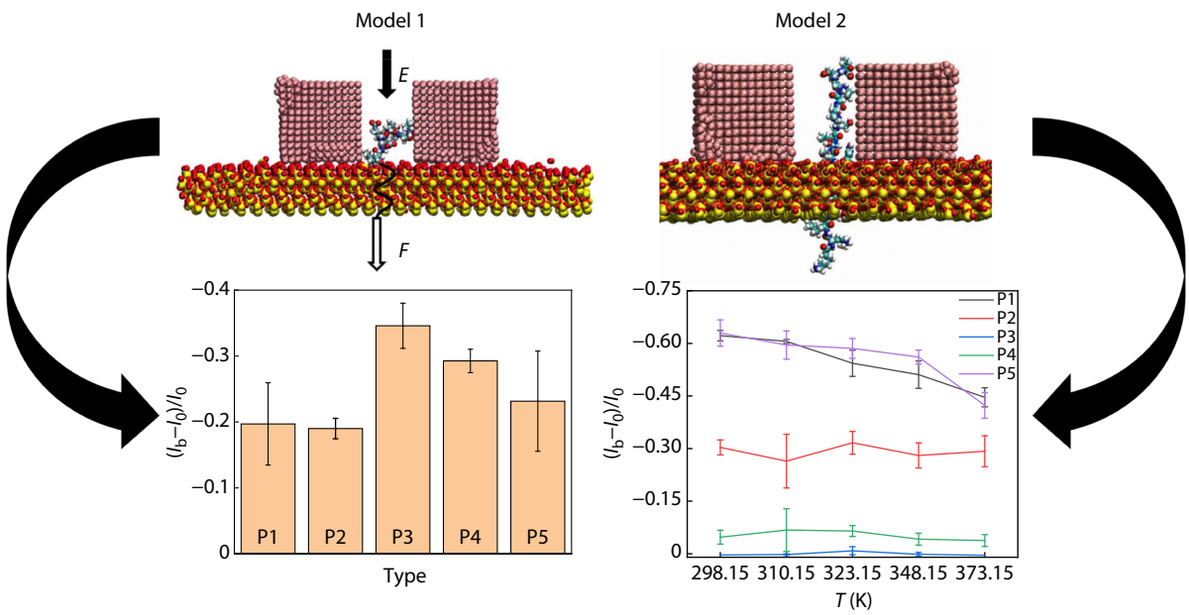
Graphical Abstract

Temperature-dependent Transport of Short Peptides through Gold Plasmonic Nanopores: the Role of Charge Heterogeneity and Residue Volume

Yi Liao, Ming-Tao Lin, and Ming-Ming Ding

Guangdong University of Technology

This study employs all-atom molecular dynamics simulations to investigate short-peptide transport through gold plasmonic nanopores. Sequence-dependent conductance blockade and dwell time arise from differences in charge distribution, residue volume, temperature response, and peptide–gold interactions, while Lys_7 conjugation facilitates electric-field-driven translocation.



Chinese J. Polym. Sci. 2026 *https://doi.org/10.1007/s10118-026-3895-z*

REFERENCES

1 Alfaro, J. A.; Bohländer, P.; Dai, M.; Filius, M.; Howard, C. J.; van Kooten, X. F.; Ohayon, S.; Pomorski, A.; Schmid, S.; Aksimentiev, A.; Anslyn, E. V.; Bedran, G.; Cao, C.; Chinappi, M.; Coyaud, E.; Dekker, C.; Dittmar, G.; Drachman, N.; Eelkema, R.; Goodlett, D.; Hentz, S.; Kalathiya, U.; Kelleher, N. L.; Kelly, R. T.; Kelman, Z.; Kim, S. H.; Kuster, B.; Rodriguez-Larrea, D.; Lindsay, S.; Maglia, G.; Marcotte, E. M.; Marino, J. P.; Masselon, C.; Mayer, M.; Samaras, P.; Sarthak, K.; Sepiashvili, L.; Stein, D.; Wanunu, M.; Wilhelm, M.; Yin, P.; Meller, A.; Joo, C. The emerging landscape of single-molecule protein sequencing technologies. *Nat. Meth.* **2021**, *18*, 604–617.

2 Brinkerhoff, H.; Kang, A. S. W.; Liu, J.; Aksimentiev, A.; Dekker, C. Multiple rereads of single proteins at single-amino acid resolution using nanopores. *Science* **2021**, *374*, 1509–1513.

3 Zhang, Y.; Yi, Y.; Li, Z.; Zhou, K.; Liu, L.; Wu, H. C. Peptide sequencing based on host–guest interaction-assisted nanopore sensing. *Nat. Meth.* **2024**, *21*, 102–109.

4 Cao, C.; Ying, Y. L.; Hu, Z. L.; Liao, D. F.; Tian, H.; Long, Y. T. Discrimination of oligonucleotides of different lengths with a wild-type aerolysin nanopore. *Nat. Nanotechnol.* **2016**, *11*, 713–718.

5 Traversi, F.; Raillon, C.; Benameur, S. M.; Liu, K.; Khlybov, S.; Tosun, M.; Krasnozhon, D.; Kis, A.; Radenovic, A. Detecting the translocation of DNA through a nanopore using graphene nanoribbons. *Nat. Nanotechnol.* **2013**, *8*, 939–945.

6 Ouldali, H.; Sarthak, K.; Ensslen, T.; Piguet, F.; Manivet, P.; Pelta, J.; Behrends, J. C.; Aksimentiev, A.; Oukhaled, A. Electrical recognition of the twenty proteinogenic amino acids using an aerolysin nanopore. *Nat. Biotechnol.* **2020**, *38*, 176–181.

7 Wang, K.; Zhang, S.; Zhou, X.; Yang, X.; Li, X.; Wang, Y.; Fan, P.; Xiao, Y.; Sun, W.; Zhang, P.; Li, W.; Huang, S. Unambiguous discrimination of all 20 proteinogenic amino acids and their modifications by nanopore. *Nat. Meth.* **2024**, *21*, 92–101.

8 Zhang, M.; Tang, C.; Wang, Z.; Chen, S.; Zhang, D.; Li, K.; Sun, K.; Zhao, C.; Wang, Y.; Xu, M.; Dai, L.; Lu, G.; Shi, H.; Ren, H.; Chen, L.; Geng, J. Real-time detection of 20 amino acids and discrimination of pathologically relevant peptides with functionalized nanopore. *Nat. Meth.* **2024**, *21*, 609–618.

9 Wang, Y.; Zhang, S.; Jia, W.; Fan, P.; Wang, L.; Li, X.; Chen, J.; Cao, Z.; Du, X.; Liu, Y.; Wang, K.; Hu, C.; Zhang, J.; Hu, J.; Zhang, P.; Chen, H. Y.; Huang, S. Identification of nucleoside monophosphates and their epigenetic modifications using an engineered nanopore. *Nat. Nanotechnol.* **2022**, *17*, 976–983.

10 Li, J.; Stein, D.; McMullan, C.; Branton, D.; Aziz, M. J.; Golovchenko, J. A. Ion-beam sculpting at nanometre length scales. *Nature* **2001**, *412*, 166–169.
11 Nicoli, F.; Verschueren, D.; Klein, M.; Dekker, C.; Jonsson, M. P. DNA translocations through solid-state plasmonic nanopores. *Nano Lett.* **2014**, *14*, 6917–6925.
12 Zhou, J.; Zhou, P. L.; Shen, Q.; Ahmed, S. A.; Pan, X. T.; Liu, H. L.; Ding, X. L.; Li, J.; Wang, K.; Xia, X. H. Probing multidimensional structural information of single molecules transporting through a sub-10 nm conical plasmonic nanopore by SERS. *Anal. Chem.* **2021**, *93*, 11679–11685.
13 Taylor, A. B.; Zijlstra, P. Single-molecule plasmon sensing: current status and future prospects. *ACS Sens.* **2017**, *2*, 1103–1122.
14 Armstrong, R. E.; Horáček, M.; Zijlstra, P. Plasmonic assemblies for real-time single-molecule biosensing. *Small* **2020**, *16*, 2003934.
15 Maccaferri, N.; Barbillon, G.; Koya, A. N.; Lu, G.; Acuna, G. P.; Garoli, D. Recent advances in plasmonic nanocavities for single-molecule spectroscopy. *Nanoscale Adv.* **2021**, *3*, 633–642.
16 Belkin, M.; Chao, S. H.; Jonsson, M. P.; Dekker, C.; Aksimentiev, A. Plasmonic nanopores for trapping, controlling displacement, and sequencing of DNA. *ACS Nano* **2015**, *9*, 10598–10611.
17 Juan, M. L.; Righini, M.; Quidant, R. Plasmon nano-optical tweezers. *Nat. Photonics* **2011**, *5*, 349–356.
18 Yang, J. M.; Pan, Z. Q.; Qin, F. F.; Chen, M.; Wang, K.; Xia, X. H. An *in situ* SERS study of ionic transport and the Joule heating effect in plasmonic nanopores. *Chem. Commun. Camb. Engl.* **2018**, *54*, 13236–13239.
19 Zhao, Y.; Hubarevich, A.; De Fazio, A. F.; Iarossi, M.; Huang, J. A.; De Angelis, F. Plasmonic bowl-shaped nanopore for Raman detection of single DNA molecules in flow-through. *Nano Lett.* **2023**, *23*, 4830–4836.
20 Reiner, J. E.; Robertson, J. W. F.; Burden, D. L.; Burden, L. K.; Balijepalli, A.; Kasianowicz, J. J. Temperature sculpting in yoctoliter volumes. *J. Am. Chem. Soc.* **2013**, *135*, 3087–3094.
21 Belkin, M.; Maffeo, C.; Wells, D. B.; Aksimentiev, A. Stretching and controlled motion of single-stranded DNA in locally heated solid-state nanopores. *ACS Nano* **2013**, *7*, 6816–6824.
22 Nam, S.; Choi, I.; Fu, C. C.; Kim, K.; Hong, S.; Choi, Y.; Zettl, A.; Lee, L. P. Graphene nanopore with a self-integrated optical antenna. *Nano Lett.* **2014**, *14*, 5584–5589.
23 Kneipp, K.; Kneipp, H.; Kartha, V. B.; Manoharan, R.; Deinum, G.; Itzkan, I.; Dasari, R. R.; Feld, M. S. Detection and identification of a single DNA base molecule using surface-enhanced Raman scattering (SERS). *Phys. Rev. E* **1998**, *57*, R6281–R6284.
24 Vanzan, M.; Migliore, A.; Blanco-Formoso, M.; De Angelis, F.; Corni, S. Mechanism of polypeptide translocation through gold nanopores in view of sequencing applications. *Nanoscale* **2026**, *18*, 5033–5051.
25 Nugraha, A. S.; Amiralian, N.; Hossain, M. S. A.; Yamauchi, Y. Nanoporous gold architectures: design, function, and emerging applications. *npj Mater. Sustain.* **2025**, *3*, 37.
26 Dey, J.; Virdi, A.; Chandra, M. Plasmon–exciton interaction at the nanoscale: silver is more "precious" than gold!. *J. Phys. Chem. Lett.* **2024**, *15*, 7674–7680.
27 Restrepo-Pérez, L.; Joo, C.; Dekker, C. Paving the way to single-molecule protein sequencing. *Nat. Nanotechnol.* **2018**, *13*, 786–796.
28 Hu, Z. L.; Huo, M. Z.; Ying, Y. L.; Long, Y. T. Biological nanopore approach for single-molecule protein sequencing. *Angew. Chem. Int. Ed.* **2021**, *60*, 14738–14749.
29 Jorgensen, W. L.; Chandrasekhar, J.; Madura, J. D.; Impey, R. W.; Klein, M. L. Comparison of simple potential functions for simulating liquid water. *J. Chem. Phys.* **1983**, *79*, 926–935.
30 Lin, M.; Zhan, L.; Ding, M. Temperature-dependent transport of charged amino acids in gold plasmonic nanopores. *J. Phys. Chem. B* **2025**, *129*, 13009–13017.
31 Wei, X.; Wen, J.; Wu, H.; Qu, Z.; Huang, G. Obtaining narrow distributions of single-molecule peptide signals enables sensitive peptide discrimination with α-hemolysin nanopores. *J. Am. Chem. Soc.* **2025**, *147*, 9304–9315.
32 Zamyatnin, A. A. Amino acid, peptide, and protein volume in solution. *Annu. Rev. Biophys. Bioeng.* **1984**, *13*, 145–165.
33 Emami, F. S.; Puddu, V.; Berry, R. J.; Varshney, V.; Patwardhan, S. V.; Perry, C. C.; Heinz, H. Force field and a surface model database for silica to simulate interfacial properties in atomic resolution. *Chem. Mater.* **2014**, *26*, 2647–2658.
34 Humphrey, W.; Dalke, A.; Schulten, K. VMD: visual molecular dynamics. *J. Mol. Graph.* **1996**, *14*, 33–38.
35 Heinz, H.; Lin, T. J.; Kishore Mishra, R.; Emami, F. S. Thermodynamically consistent force fields for the assembly of inorganic, organic, and biological nanostructures: the INTERFACE force field. *Langmuir* **2013**, *29*, 1754–1765.
36 Miyamoto, S.; Kollman, P. A. Settle: an analytical version of the SHAKE and RATTLE algorithm for rigid water models. *J. Comput. Chem.* **1992**, *13*, 952–962.
37 Batcho, P. F.; Case, D. A.; Schlick, T. Optimized particle-mesh Ewald/multiple-time step integration for molecular dynamics simulations. *J. Chem. Phys.* **2001**, *115*, 4003–4018.
38 Berendsen, H. J. C.; Postma, J. P. M.; van Gunsteren, W. F.; DiNola, A.; Haak, J. R. Molecular dynamics with coupling to an external bath. *J. Chem. Phys.* **1984**, *81*, 3684–3690.
39 Bussi, G.; Donadio, D.; Parrinello, M. Canonical sampling through velocity rescaling. *J. Chem. Phys.* **2007**, *126*, 014101.
40 Belkin, M.; Aksimentiev, A. Molecular dynamics simulation of DNA capture and transport in heated nanopores. *ACS Appl. Mater. Interfaces* **2016**, *8*, 12599–12608.
41 Aksimentiev, A.; Heng, J. B.; Timp, G.; Schulten, K. Microscopic kinetics of DNA translocation through synthetic nanopores. *Biophys. J.* **2004**, *87*, 2086–2097.
42 Aksimentiev, A.; Schulten, K. Imaging alpha-hemolysin with molecular dynamics: ionic conductance, osmotic permeability, and the electrostatic potential map. *Biophys. J.* **2005**, *88*, 3745–3761.
43 Zhang, Y. S.; Qi, Z. Y.; Ding, M. M.; Li, M. L.; Shi, T. F. Translocation of ssDNA through charged graphene nanopores: effect of the charge density. *Chinese J. Polym. Sci.* **2024**, *42*, 2048–2058.
44 Zhang, Y.; Ding, M. Probing nanopores: molecular dynamics insights into the mechanisms of DNA and protein translocation through solid-state and biological nanopores. *Soft Matter* **2025**, *21*, 2385–2399.
45 Yan, S.; Zhang, J.; Wang, Y.; Guo, W.; Zhang, S.; Liu, Y.; Cao, J.; Wang, Y.; Wang, L.; Ma, F.; Zhang, P.; Chen, H. Y.; Huang, S. Single molecule ratcheting motion of peptides in a *Mycobacterium smegmatis* porin a (MspA) nanopore. *Nano Lett.* **2021**, *21*, 6703–6710.
46 Chen, Z.; Wang, Z.; Xu, Y.; Zhang, X.; Tian, B.; Bai, J. Controlled movement of ssDNA conjugated peptide through *Mycobacterium smegmatis* porin A (MspA) nanopore by a helicase motor for peptide sequencing application. *Chem. Sci.* **2021**, *12*, 15750–15756.
47 Chen, Z.; Wang, J.; Meng, X.; Ye, F.; Wang, L.; Xu, Y.; Wang, X.; Wang, Q.; Wen, H.; Bai, J. Spike signals and MD simulations reveal the significance of peptide stretching in nanopore protein sequencing. *J. Am. Chem. Soc.* **2025**, *147*, 24347–24359.
48 Hu, F.; Angelov, B.; Li, S.; Li, N.; Lin, X.; Zou, A. Single-molecule study of peptides with the same amino acid composition but different sequences by using an aerolysin nanopore. *ChemBioChem* **2020**, *21*, 2467–2473.

https://doi.org/10.1007/s10118-026-3895-z